



Published in final edited form as:

*Conf Proc IEEE Eng Med Biol Soc.* 2012 ; 2012: . doi:10.1109/EMBC.2012.6347236.

## A pipeline for the Simulation of Transcranial Direct Current Stimulation for Realistic Human Head Models using SCIRun/BioMesh3D

Moritz Dannhauer<sup>1</sup>, Dana Brooks<sup>2</sup>, Don Tucker<sup>3,4</sup>, and Rob MacLeod<sup>1</sup>

Moritz Dannhauer: moritz@sci.utah.edu

<sup>1</sup>Scientific Computing and Imaging Institute, 72 So. Central Campus Drive, Salt Lake City, Utah 84112, USA

<sup>2</sup>Department of Electrical and Computer Engineering 409 Dana Center, 360 Huntington Avenue, Boston, MA 02115, USA

<sup>3</sup>Department of Psychology, Clinical Cognitive Neuroscience, University of Oregon

<sup>4</sup>Electrical Geodesics, Inc., Riverfront Research Park, 1600 Millrace Drive, Suite 307, Eugene, OR 97403, USA

### Abstract

The current work presents a computational pipeline to simulate transcranial direct current stimulation from image based models of the head with SCIRun [15]. The pipeline contains all the steps necessary to carry out the simulations and is supported by a complete suite of open source software tools: image visualization, segmentation, mesh generation, tDCS electrode generation and efficient tDCS forward simulation.

### I. INTRODUCTION

Transcranial direct current stimulation (tDCS) aims to stimulate certain brain regions by sending constant low direct currents non-invasively through electrodes that are usually attached to the scalp. It has been known for over 100 years but has just recently become popular as a tool in brain research ([1], [16], [4]) as well as in therapy to support treatments of psychological disorders ([4]). While the focus of the results reported here work is tDCS, there are other non-invasive techniques that are widely used for neuronal stimulation such as transcranial magnetic stimulation (TMS) in which electrical current are magnetically induced. During the application of both TMS and tDCS other unwanted regions are stimulated at the same time and there has been some research to minimize the unwanted activity in those brain regions ([7]). The goal of the present study was develop and validate a computational pipeline capable of optimize electrode configurations and current injection patterns to stimulate only specific desired brain regions.

In tDCS simulations, the *tDCS forward problem* that has to be solved requires a geometric model of the head, typically from medical image data, as a volume conductor for a realistic modeling of electrical field propagation. In general, this electrical field propagation (volume conduction) depends mainly on tissue conductivities which are only roughly known *in-vivo* for many of the involved tissues (e.g. skull, skin, grey and white matter of the brain, cerebrospinal fluid (CSF), etc.). As the volume conductor consists of a discrete approximation of the actual head, the resolution of the model and the configuration of the interfaces between the surfaces play important roles in numerical accuracy of the solutions. Certainly, one of the most important tissues in electrical head modeling is the poorly conducting skull tissue which forms an electrical barrier between the brain and the surface

electrodes. Skull modeling is important since the conductivity profile depends very much on the local presence of differently conducting skull tissues which are inhomogeneously distributed within the skull ([6]). In order to integrate those different skull tissues (soft and hard bone) in the model they first have to be identified from the medical images. One way to differentiate them is to decide whether or not a voxel belongs to one or another material based on thresholding the grey values from computed tomography (CT) images. Once the material of a voxel is properly identified a more or less accurate conductivity value is assigned to it (see section below on conductivities) as well as to the associated elements in the model mesh. For a fully realistic tDCS forward solution tissue inhomogeneity in the skull and anisotropic conductivity in the white matter of the brain should be considered ([18]) and be part of the computational pipeline and the final model.

With the volume conductor model in place, there are common ways to solve the tDCS forward problem numerically, for example the Finite Difference Method, as well as the Finite Element Method (FEM, e.g. [19]). FEM is very flexible in dealing with tissue inhomogeneities, irregular tissue boundaries, and conductivity anisotropy and was therefore the numerical method of choice for this study.

In tDCS, the location and shape of the electrodes ([13]) as well as details of the applied current injection (e.g. contact impedance, [9]) play an important role for electrical field propagation and the accuracy of the simulation. There are several electrode models in the literature (e.g. shunt, complete, [5], [13], [2]) in which different electrical boundary conditions are applied together with certain assumptions about the electrode-surface interaction. In realistic settings, and in this study, the complete electrode model is often used since it also includes realistic contact impedances ([5]).

We present a pipeline to compute tDCS simulations for realistic volume conductor models using a combination of open source software tools that includes ImageVis3D, Seg3D, BioMesh3D and SCIRun, all products of the NIH Center for Integration Biomedical Computing ([www.sci.utah.edu/cibc](http://www.sci.utah.edu/cibc)). For exhaustive tDCS simulations, e.g. for the optimization of electrode configurations and injection current patterns, a technique called *transfer matrix approach* ([17]) can be used to reduce the computational effort.

## II. Methods

For demonstration purposes of the pipeline (see figure 1) we use an example scenario.

### A. Anatomical Imaging

To generate a realistic anatomical model, image data sets were acquired from a human subject using both a T1-weighted magnetic resonance image (MRI) and computed tomography (CT) data set (at 1x1x1 mm voxel resolution).

### B. Segmentation and Registration

The segmentation of the skull tissue was performed by using an absolute threshold method for the CT data set to separate air filled cavities and the skull tissues. For the identification of grey- and white matter from MRI we used a relative threshold method. The segmentation of the different tissues from both imaging modalities (CT, MRI) were registered in a semi-automatic way using Brain Voyager ([3]) and custom code written in Matlab ([11]). The final segmentation contained the following tissues: skin, eyes, skull, CSF, grey and white matter from the brain, internal air and electrode material.

In order to minimize distortions originating from dental fillings located in some axial slices (close to the mouth) those slices had to be carefully checked and manually corrected.

Further, the surfaces of those areas were smoothed to create an anatomical plausible and esthetical pleasing appearance of the head (spatial 3D gauss filter (vgauss3d, lipsia package, [10]). Furthermore, to ensure anatomical plausibility, e.g. to avoid procedure-based artifacts such as holes in the skull, several additional preprocessing steps were performed (e.g. dilate/erode/fill holes and manual correction of falsely classified skull voxels).

### C. Electrodes

Typical applications of tDCS make use of large (several centimeter squared) patch-like electrodes. However, there are advantages to using instead a set of smaller electrodes wired together. Each electrode is more likely to establish good skin contact and the configuration and shape of each constructed patch is much easier to control and even adjust on patient specific basis. Hence we set out to evaluate the relative performance of true patch electrodes compared to a constructed patch from multiple, smaller electrodes. Each electrode from a 128-electrode flexible mesh (EGI, Geodesic Sensor Inc.) was attached to the skin via a sponge soaked-up in saline and held in place through gentle tension in the electrode mesh. The sponge had a cylindrical shape with a diameter of 12 mm and a height of 5 mm that were explicitly integrated into the segmentation. This technique guaranteed that the contact surface between sponge and skin surface was naturally shaped and properly sampled.

### D. Meshing - Biomech3D

Biomech3D is a mesh generator package that uses a variational meshing optimization in which the entropy of the surface particals over the surface so as to produce optimally spaced vertices ([12]). This method allows for local refinement in a way that represents with additional particles areas of high curvature or very thin features. The algorithm also allows for multi-material models even with very complex or non-manifold structures, which are commonly found in biological data.

The meshing of this complex head model took 3 days using a single-threaded version of BioMesh3D. In upcoming releases of BioMesh3D there will be a parallelized version available (multi-threads, GPU) which reduces the time consumption to a few hours. The final mesh in this study contained  $N = 6,662,239$  mesh nodes and 38,212,880 tetrahedral elements (figure 2).

### E. Isotropic Conductivities

For each tetrahedral element, isotropic conductivities were assigned based on the segmentation labels and literature conductivity values as follows: skin (0.43 S/m, [8]), hard skull bone (0.0064 S/m, [6]), soft skull bone (0.02865 S/m, [6]), CSF (1.79 S/m, [8]), brain's grey matter (0.33 S/m, [8]), brain's white matter (0.142 S/m, [8]), eyes (0.17 S/m, [8]), internal air (0.0001 S/m, [8]) and saline (0.367 S/m, [14]).

### F. tDCS Forward Matrix

For the purpose of computing the tDCS forward solution (defined in tDCS matrix  $M$ , see figure 3) the following equation system has to be solved for the potential vector  $U$  given a current density  $I$  such as,

$$MU=I \Rightarrow U=M^{-1}I.$$

The tDCS matrix  $M$  is composed of the FEM stiffness matrix ( $A \in N \times N$ ) and additional electrical boundary condition matrices ( $B \in N \times E$ ,  $C \in E \times E$ ).

$$\begin{aligned}
 M &= \begin{pmatrix} A & -B \\ -B^T & C \end{pmatrix} \\
 \begin{pmatrix} A & -B \\ -B^T & C \end{pmatrix} \begin{pmatrix} u_n \\ u_e \end{pmatrix} &= I = \begin{pmatrix} i_n \\ i_e \end{pmatrix} \\
 A(i, j) &= \int_D \sigma \nabla \varphi_i \cdot \nabla \varphi_j dD + \sum_{l=1}^L \frac{1}{z_l} \int_{e_l} \varphi_i \varphi_j dD_{el} \\
 B(i, j) &= \frac{1}{z_l} \int_{e_l} \varphi_i dD_{el} \\
 C(l, l) &= \frac{1}{z_l} \int_{e_l} dD_{el}
 \end{aligned} \quad (1)$$

with

$$\begin{aligned}
 M &= \text{FEM stiffness matrix} + \text{boundary conditions } M \in \mathbb{R}^{m+L \times m+L}, l=1..L \\
 U &= \text{Potentials at nodes} \\
 I &= \text{Currents at nodes} \\
 D &= \text{FEM domain} \\
 \varphi &= \text{Linear basis function} \\
 e_l &= \text{lth electrode} \\
 L &= \text{Number of electrodes} \\
 z_l &= \text{Contact impedance of lth electrode} \\
 A, B, C &= \text{Boundary conditions}
 \end{aligned} \quad (2)$$

The boundary conditions are defined as integrals over the linear basis functions defined on the finite elements which have analytical solutions. In our case those basis functions are defined on tetrahedral elements and have the following analytical solutions ( $V$  being the volume of each tetrahedra),

$$\begin{aligned}
 \int_{e_l} D_{el} &= V \\
 \int_{e_l} \varphi_i dD_{el} &= \frac{1}{4} V \\
 \int_{e_l} \varphi_i \varphi_i dD_{el} &= \frac{1}{10} V \\
 \int_{e_l} \varphi_i \varphi_j dD_{el} &= \frac{1}{20} V.
 \end{aligned} \quad (3)$$

The method to compute the tDCS matrix  $M$  (complete electrode model) is implemented as a SCIRun module (see figure 3) for point electrodes, 2D patch electrodes (triangles) and 3D electrodes (tetrahedra) (see figure 3). To speed up the computations for exhausting simulations the transfer matrix approach is implemented in SCIRun (see figure 4) to solve the potential distribution for unit currents injected at the electrodes ( $i_e$ ).

## G. Simulation

Two electrodes were chosen to demonstrate the simulation of a current source (blue) and a current sink (red) of about  $\pm 1$  mA, see the tDCS forward solution in figure 5 and 6.

## III. Results

In figure 2, the meshing results for skin, electrodes and skull are visualized. It can be seen that those smoothed surfaces (BioMesh3D) reflect a very detailed human head anatomy. Figure 3,4 show the SCIRun nets used to compute the tDCS forward solution and the transfer matrix.

In figure 5 and 6 the tDCS forward solution ( $U$ ) is depicted on the skin as well as on the cortical surface. The computation of the needed columns (for the two electrodes) in the transfer matrix took about 20 minutes. Furthermore, the computation time highly depends on the required numerical accuracy. We used a residual error norm of  $10^{-9}$  as convergence criteria and it was apparent that the convergence also depended on the used surface impedance (here  $50 \text{ k}\Omega$ ). The smaller (compared to skin resistance) the surface impedance the faster the convergence of conjugate gradient solver likely due to the fact that most of the mesh nodes had a potential of zero if the surface impedance was smaller than the skin resistance. After that, the actual forward solution was just a linear combination of both columns and takes only a few milliseconds to compute. Therefore, tDCS forward simulations can generally be done extremely quickly using the transfer matrix approach.

## IV. Conclusion

The proposed pipeline was capable of generating realistic head models for FEM simulations using an adaptive meshing approach (BioMesh3D). The implemented SCIRun modules were able to model arbitrary shapes of electrodes and configurations as well as realistic boundary conditions specified by the complete electrode model. Compared to other software packages (e.g. Eiders3D) our pipeline also supports the modeling of anisotropic conductivity tensors/properties (e.g. for white matter and skull modeling) and arbitrary electrode shapes and configurations. To speed-up simulations the transfer matrix approach was implemented using a highly parallelized conjugate gradient solver.

## Acknowledgments

This work was not supported by any organization

The authors want to thank the following people for their contributions: Chelsea Mattson, Sergei Turvets, Darrell Swenson, Seyhmus Güller and Kathrin Rothermich.

## References

1. Benninger DH, Lomarev M, Lopez G, Wassermann EM, Lui X, Considine E, Hallett M. Transcranial direct current stimulation for the treatment of Parkinson's disease. *J Neuro Neurosurg Psychiatry*. 2010
2. Boyle A, Adler A. Electrode Models under Shape Deformation in Electrical Impedance Tomography. *J Phy Conf Ser*. 2010; 224
3. Goebel R. BrainVoyager - Past, present, future. *NeuroImage*. 2012 [Epub ahead of print].
4. Brunoni AR, Ferruci R, Bortolomasi M, Vergari M, Tadini L, Boggio PS, Giacomuzzi M, Barbieri S, Priori A. Transcranial direct current stimulation (tDCS) in unipolar vs. bipolar depressive disorder. *Prog Neuropsychopharmacol Biol Psychiatry*. 2011; 35(1):96–101. [PubMed: 20854868]
5. Cheng KS, Newell JC. Electrode Models for Electrical Current Computed Tomography. *IEEE TRANSACTIONS ON BIOMEDICAL ENGINEERING*. 1989; 36(9)
6. Dannhauer M, Lanfer B, Wolters CH, Knösche TR. Modeling of the human skull in EEG source analysis. *Human Brain Mapping*. 2011; 32(9):1383–1399. [PubMed: 20690140]
7. Dmochowski JP, Datta A, Bikson M, Su Y, Para LC. Optimized multi-electrode stimulation increases focality and intensity at target. *J Neural Eng*. 2011; 8
8. Haueisen J, Ramon C, Eiselt M, Brauer H, Nowak H. Influence of Tissue Resistivities on Neuromagnetic Fields and Electrical Potentials Studied with a Finite Element Model of the Head. *IEEE TRANSACTIONS ON BIOMEDICAL ENGINEERING*. 1997; 44(8)
9. Hua P, Woo EJ, Webster JG. Finite Element Modeling of Electrode-Skin Contact Impedance in Electrical Impedance Tomography. *IEEE TRANSACTIONS ON BIOMEDICAL ENGINEERING*. 1993; 40(4)

10. Lohmann G, Miller K, Bosch V, Mentzel H, Hessler S, Chen L, Zysset S, von Cramon DY. LIPSIA - a new software system for the evaluation of functional magnetic resonance images of the human brain. *Computerized Medical Imaging and Graphics*. 2001; 25(6):449–457. [PubMed: 11679206]
11. MATLAB version 7.12.0. Natick, Massachusetts: The MathWorks Inc; 2011.
12. Meyer M, Whitaker R, Kirby RM, Ledergerber C, Pflister H. Particle-based Sampling and Meshing of Surfaces in Multimaterial Volumes. *IEEE TRANSACTIONS ON VISUALIZATION AND COMPUTER GRAPHICS*. 2008; 14(6)
13. Pursiainen S, Lucka F, Wolters CH. Complete electrode model in EEG: relationship and differences to the point electrode model. *Phys Med Biol*. 2012; 57:999. [PubMed: 22297396]
14. Babaeizadeh S, Brooks DH. Electrode Boundary Conditions and Experimental Validation for BEM-Based EIT Forward and Inverse Solutions. *IEEE TRANSACTIONS ON MEDICAL IMAGING*. 2006; 25(9)
15. SCIRun+BioMesh3D: A Scientific Computing Problem Solving Environment, Scientific Computing and Imaging Institute (SCI). 72 So. Central Campus Drive, Salt Lake City, Utah 84112, USA: web: <http://www.sci.utah.edu/software/biomesh3d.html>, <http://www.sci.utah.edu/software/scirun.html>
16. Vandermeeren Y, Jamart J, Ossemann M. Effect of tDCS with an extracephalic reference electrode on cardiorespiratory and autonomic functions, 2010. *BMC Neurosci*. 11:38. [PubMed: 20233439]
17. Woltes CH, Grasedyck L, Hackbusch W. Efficient computation of lead field bases and influence matrix for the FEM-based EEG and MEG inverse problem. *Inverse Problems*. 2004; 20:1.
18. Wolters CH, Anwander A, Tricoche X, Weinstein D, Koch MA, MacLeod R. Influence of Tissue Conductivity Anisotropy on EEG/MEG Field and Return Current Computation in a realistic Head Model: A Simulation and Visualization Study using High-Resolution Finite Element Modeling. *NeuroImage*. 30(3):813–826. [PubMed: 16364662]
19. Wolters CH, Köstler H, Möller C, Härdtlein J, Grasedyck L, Hackbusch W. Numerical Mathematics of the Subtraction Method For the Modeling of a Current Dipole in EEG Source Reconstruction Using Finite Element Head Models. *SIAM J SCI Comput*. 20

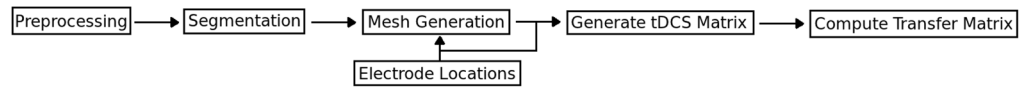


**Fig. 1.** Pipeline for efficient tDCS simulation - each step in the pipeline represents one or more software tools that are integrated into a flexible, efficient workflow.

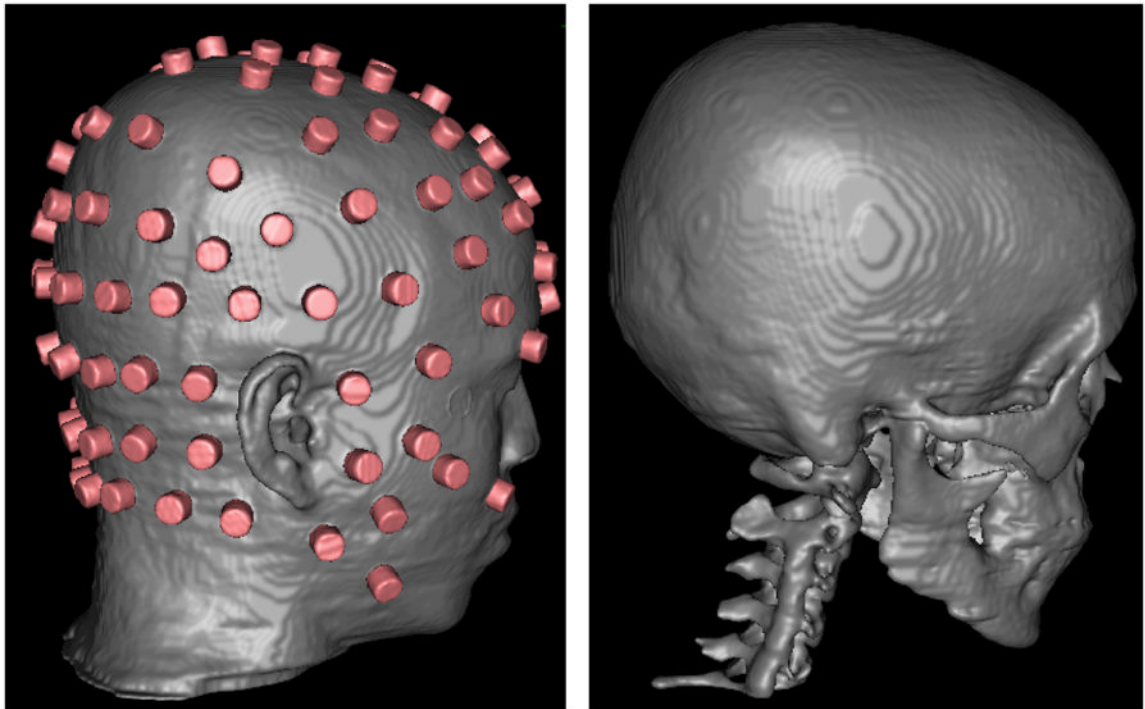


**Fig. 2.**  
Mesh: (left) skin+electrodes (right) skull

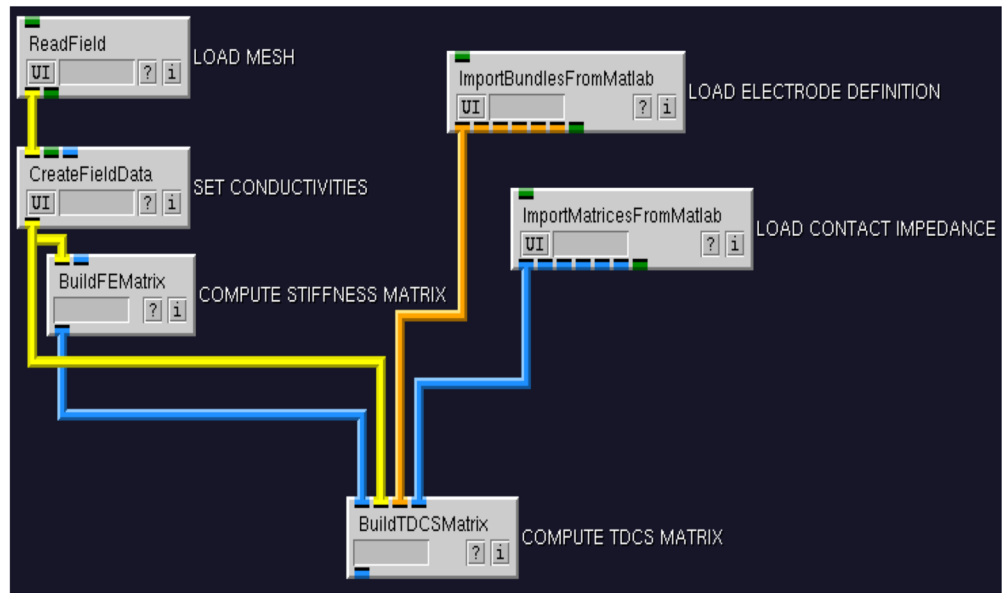


**Fig. 3.**  
tDCS Matrix computation

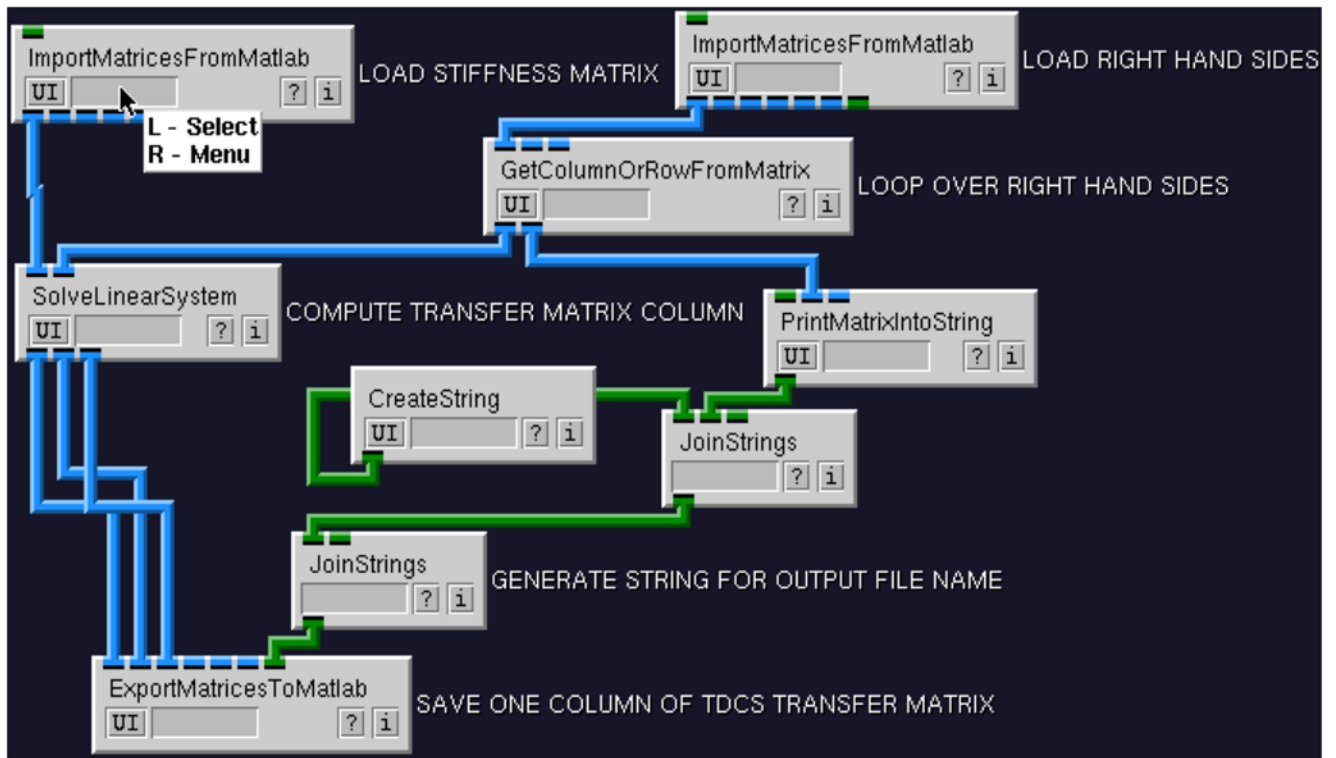


**Fig. 4.**  
Transfer Matrix computation

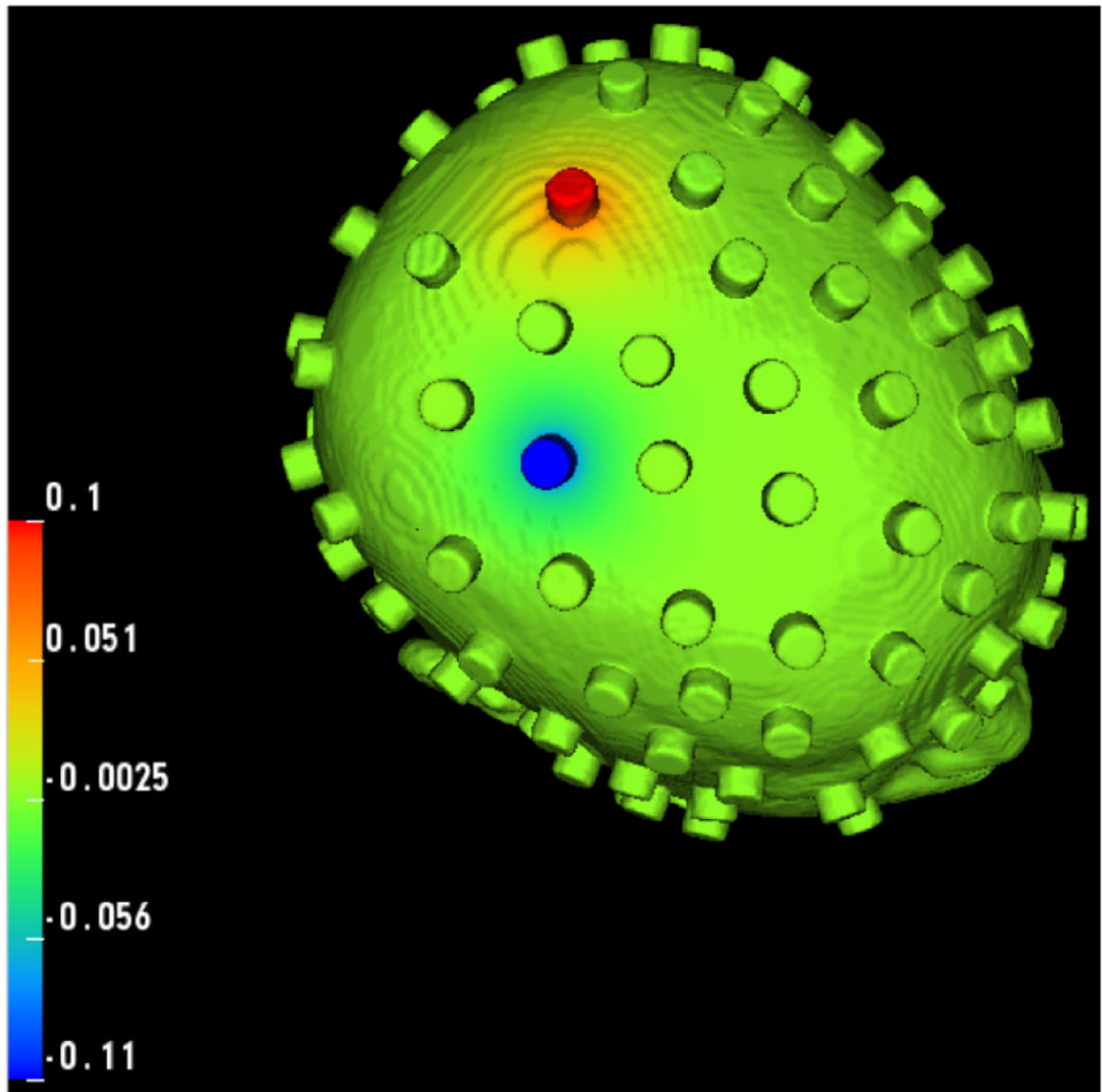


Fig. 5.  
tDCS injected potential ( $\mu V$ ) distribution on skin surface

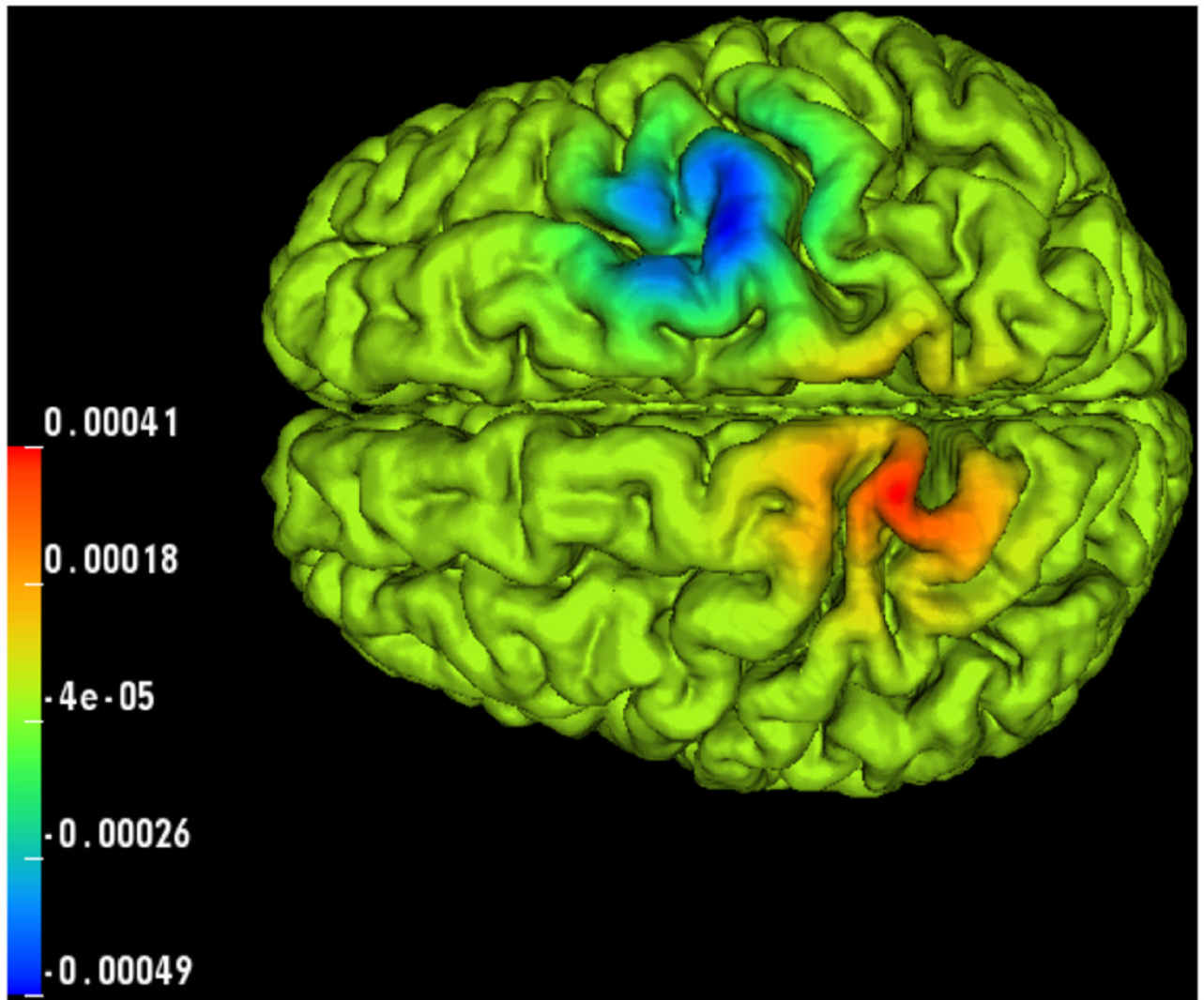


Fig. 6.  
tDCS injected potential ( $\mu V$ ) distribution on brain surface